A theory that predicts behaviors of disordered cytoskeletal networks

Julio Belmonte, Maria Leptin and François Nédélec

SUPPLEMENTARY MATERIAL

We describe here first the details of the networks studied and the hypotheses under which our research was conducted. We then summarize the approach and specific parameters of simulations used to verify the theory, which are based on previously published methods and open source public software (Cytosim). Finally, to illustrate both the theory and the simulations, we present the analysis of a system where bi-functional motors and passive crosslinkers act on a network of stabilized filaments. For this example, the theory makes a quantitative prediction of how the contraction rate depends on the numbers of connectors acting between the filaments. This approach is general, and can be adapted to predict the behavior of networks with any combination of all of the possible types of active connectors.

Table of contents:

A. General Assumptions

We describe here the general hypotheses of our study. In brief, we considered idealized disordered networks of semi-flexible polar filaments, simplified to retain only those elements that appear essential for contraction. Filaments are infinitely thin, and their degrees of freedom represent position, orientation and bending, but longitudinal extension and twist around the axis are ignored. A network is made of thousands of filaments, positioned and oriented randomly in all

directions thus constituting an isotropic and uniform meshwork. The filaments have a fixed length and no assembly or disassembly occurs at their ends. All the filaments have the same length and this length is shorter than the diameter of the network. We ignore edge effects as much as possible, to focus on the average behavior deep within the network.

The **filaments** are either *rigid* or *semi-flexible*, meaning that the length of the filaments is shorter than their persistence length. We expect this condition to hold true for cytoskeletal networks encountered in reality, since the persistence length is ~18μm for F-actin and ~5000μm for microtubules. We assume that the network is initially free of strain, implying that since they are shorter than their persistence length, the filaments should be nearly straight.

Different types of **connectors** link the filaments together. Each connector is composed of two filament-binding subunits, and acts as a mechanical link between two filaments of the network. Subunits differ in two ways: i) by the position on filaments to which they can bind; and ii) by whether they can travel along the filament or not. We call a subunit that does not move a *binder,* and a subunit that moves a *motor*. "End-binders" are subunits that can only bind near the end of the filaments and do not move. 15 different types of connectors can be made from the 5 possible different subunits, and, for many of them, examples are found in living cells. For example, cross-linkers like alpha-actinin or filamin can be represented by a connector with identical binders that can bind anywhere along the filament; while bi-functional motors, such as members of the kinesin-5 family, Myosin IV motor proteins or dynein complexes are represented by connectors with two motor subunits that can bind anywhere along the filament. For simplicity, we assume that connectors do not interfere with each other, and that the subunits of connectors are non-interacting in the bound state. There is no limitation on the number of connectors that may bind to a filament. The motion of **motors** along a filament is unobstructed. Their velocity depends on force, but their detachment rate does not. A motor detaches immediately upon reaching the end of the filament on which it is travelling. A connector has no drag resistance and exerts opposite forces on the two points to which it is attached.

The system is characterized by a very low Reynolds number[1], and inertia of the object can be neglected. Moreover, we are here interested chiefly in the behavior of the system determined by the forces transmitted by the connectors and by the bending elasticity of the filaments. We thus focus on the regime where there are enough connectors to create a coherent mechanical ensemble. Filaments should be linked in such a way that the major factor that limits the extent to which forces are transmitted across the network is the filament bending elasticity, rather than the elasticity of the connections. We thus assumed that the connectors are short compared to the filaments, and remain so even when under tension. We find this the most interesting regime to study, since it should correspond to the one that is able to develop the strongest forces.

Because we intend to simulate thin networks such as the actin cortex underlying the plasma membrane, where the filaments are nearly parallel to the plasma membrane, all simulations were performed in 2D. We also ignored direct steric interactions and hydrodynamic coupling between the filaments. The motion of the filaments is thus determined by diffusion, and by constraints imposed by the connections between filaments. Under these assumptions, the microscopic

motions of active connectors, which have a motor as one or both of their subunits, induce forces that lead to the overall deformation of the network. Passive connectors, although they do not generate forces themselves, have an essential role in transmitting the force generated by the motors. Our theory is based on the assumption that averaging over the many possible microscopic configurations of these elements will predict the bulk initial behavior of the entire system. We used Cytosim-based simulations[2] using the conditions described in this section, to test this prediction.

B. Description of the Simulations

The way in which a model network evolves was calculated using Cytosim, a software platform developed to model systems of flexible cytoskeletal fibers that are connected by different types of molecules[2]. Cytosim is an open source project hosted on GITHUB (http://github.com/nedelec/cytosim). The algorithms of Cytosim efficiently solve the Brownian dynamics of the filaments, and the stochastic binding and unbinding of their associated molecules. Briefly, the Brownian dynamics of a point-like object is defined by an over-damped Langevin equation: $\xi \frac{dx}{dt} = f(x,t) + B(t)$, for a vector position x, where the right-hand terms are the deterministic and random forces respectively, and ξ is a drag coefficient typically calculated using Stokes' law from the viscosity of the fluid and the size of the object. Such an equation accurately describes the motion of a micrometer-sized bead in a fluid that has the viscosity of cytoplasm. The filaments are elongated objects, discretized with "model-points" distributed regularly along their length (Fig. 3A). A large multivariate differential equation involving the coordinates of all the model-points is constructed and solved using a first-order implicit numerical integration scheme [2]. Although of higher dimensionality, this equation remains in essence similar to the equation presented here to model the motion of a single bead. In addition to Brownian motion in each point of the filament, the equation includes the bending elasticity of the filaments and the forces generated by the connectors (Fig. 3A). The implicit scheme makes it possible to integrate the system with a time-step of a few milliseconds, leading to a significant performance gain over explicit integration schemes, for which time steps possibly in the micro-second range must be used. Cytosim moreover uses algebraic constraints to ensure that the length of the filament remains constant, such that filaments are incompressible and inextensible, which seems physically appropriate for cytoskeletal filaments, considering the magnitude of the forces generated by molecular motors. For instance, the stretching elasticity of a single 1 μm-long actin filament was reported to be 35 pN/nm [3], corresponding to an elongation of 0.01% under the approximate force produced by one myosin motor.

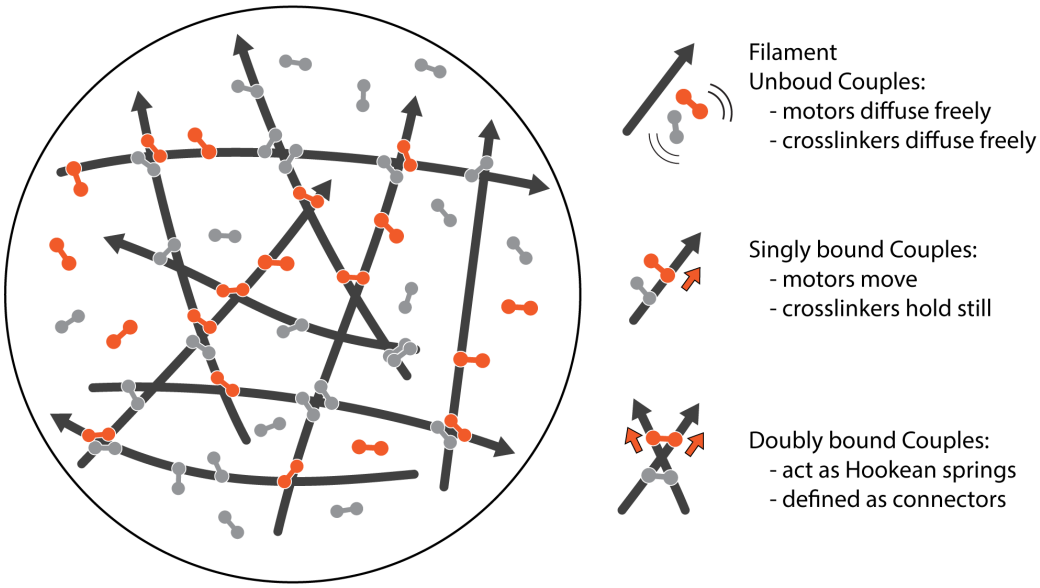

Figure S1: Schematic of 2D network of filaments simulated in Cytosim. The filaments are polar and flexible. We used a Cytosim object called "Couples" to represent motors and crosslinkers. A Couple is composed of two filament-binding activities and is able to make dynamic connections between neighboring filaments. In this example, motors and crosslinkers are composed of two identical subunits, and can be found in 3 different states: unbound, singly bound or doubly bound. Only Couples that are doubly bound can influence the mechanics of the system, and are thus connectors of the network. In Cytosim, they are mechanically represented by Hookean springs. The doubly bound motors are the only types of active connectors that can drive the contraction or extension of the network.

While in the theory we introduced the term of "Connector" to refer to a mechanical link between two filaments, Cytosim uses the term "*Couple*" for an object composed of two independent activities (Fig. S1). Connectors and Couples are different concepts. Each subunit of a Couple can dynamically bind to and unbind from filaments, with predefined and constant rates (Fig. 3B,C,G). Binding and unbinding are first-order stochastic processes. The two subunits of a Couple behave independently, except that they cannot both be bound to nearby positions on one filament. At any given time, some of the Couples are unbound, some are bound to only one filament, and some are bound to two filaments. The three sub-species are in equilibrium. Only the Couples attached to two filaments induce force, and can thus be considered as Connectors in the theory. Such connectors create Hookean springs with a zero resting-length. The associated stiffness (K) is a parameter of the simulation, and was set for this study sufficiently high to disallow the motors to extend significantly. Unbound Couples diffuse freely within the network, and may bind to any filament closer than their reach (ε) with a constant binding rate (k_{on}). Singly bound Couples unbind with a constant rate (k_{off}), and may bind to a second filament if it is within reach (ε), with the same rate (k_{on}). Doubly bound Couples may unbind from either subunit, doubling the effective unbinding rate ($2k_{off}$). In this work, the force that is present in the link of a doubly bound Couple is not taken into account to calculate the unbinding rate. Under these simple assumptions, it is possible to predict the fraction of the Couples found in each configuration when equilibrium is reached (see part D). The force of a doubly bound motor reduces the speed of the motor linearly as $v = v_m\left(1 - \frac{f}{f_s}\right)$, where v_m is the unloaded speed of the motor, f_s is the stall force, and f is the

component of the force parallel to the filament, taken to be positive if the force is antagonizing the spontaneous motion of the motor.

For all the simulations described in this study, the system was first equilibrated, both in terms of mechanical configuration of the filaments, and Couple binding-unbinding kinetics for a sufficient time to reach equilibrium (typically 4 seconds of "simulated time"). During this time, the motors are not allowed to move (speed=0) and the system is passive. After equilibration, the motors are "activated", by setting the unloaded speed as desired, and the simulation is continued for a sufficient period of "simulated time" to estimate the network's contraction rate.

C. Extraction of the Contraction Rate from Simulations

To be able to compare the performance of networks with different sets of parameters we determined a numerical value for the contraction rate. The contraction rate of the network is calculated as the difference in "network radius" divided by elapsed time. To estimate the network size, we first calculated the center of mass c as:

$$c = \frac{1}{P}\sum_i x_i$$

where the positions x_i of all the points used to represent filaments in the system are averaged (P is the total number of model points in the system). The size of the network is then calculated as:

$$R = \sqrt{\frac{2}{P}\sum_i (x_i - c)^2}$$

This is a simple and robust measure of network size, and if the filaments are uniformly distributed over a disc of radius Q, then $R \sim Q$. Thus, R is an indicator of the radius of the round area covered by a network, which contracts or expands isotropically (Fig. S2).

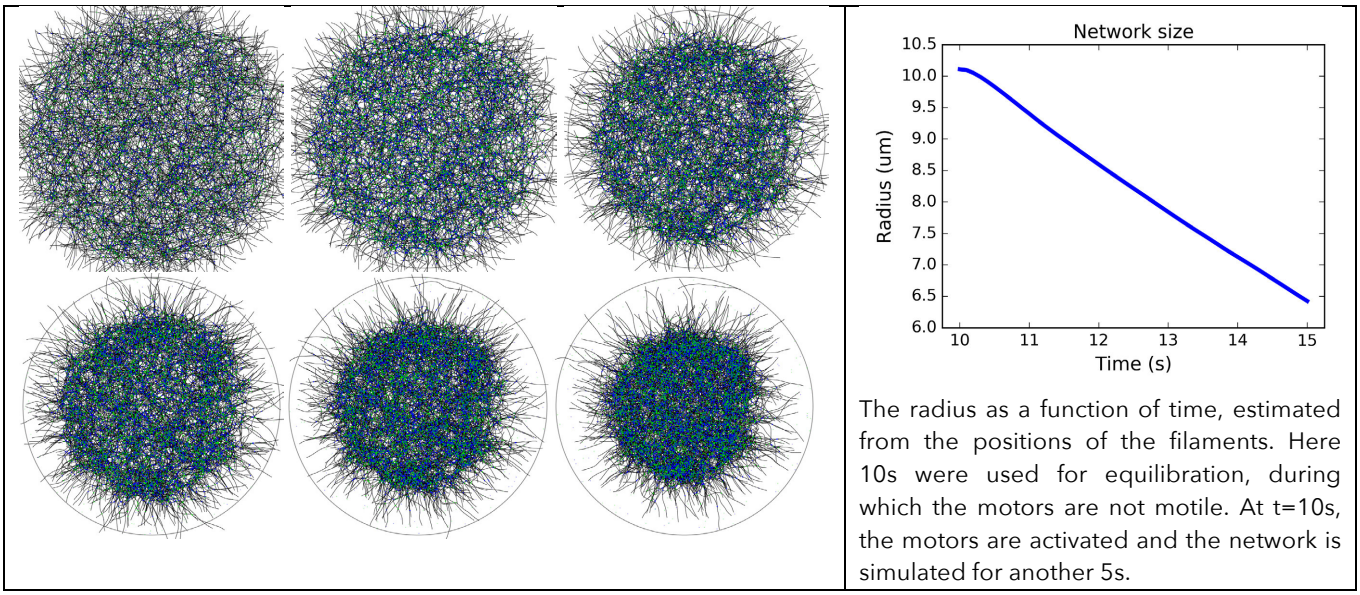

The radius as a function of time, estimated from the positions of the filaments. Here 10s were used for equilibration, during which the motors are not motile. At t=10s, the motors are activated and the network is simulated for another 5s.

Figure S2: Contraction of a network composed of 2000 filaments initially distributed over a disc of radius 10 μm. The length of the filaments is 5 μm, and the system contains 8141 motors and 9295 crosslinkers. Snapshots are separated by intervals of 1s. The extracted size of the network, as defined by the formula described above, is plotted on the right. The radius as a function of time is nearly linear, and the contraction rate (the slope) is well defined.

The contraction rate of the network, which has units of μm/s, is then simply estimated as a finite difference between two time points:

$$\frac{dR}{dt} = \frac{R(t_2) - R(t_1)}{t_2 - t_1}$$

For all simulations, we allow some relaxation time before calculating the contraction rate, but the contraction rate is usually stable over a period of 5 seconds. At longer times, the contraction rate diminishes exponentially (data not shown). Negative values of dR/dt indicate that the system is contracting, while positive values reflect expansion.

D. Analysis of the Contraction Rate with Motors and Crosslinkers

We now go through the specific example that we used to develop the theory. We proceeded by comparing analytical predictions against the outcomes of simulations in cytosim. We choose a 2D network, and two types of Couples made of two identical subunits: a bi-functional motor and a bi-functional passive binder. This is the most widely studied synthetic system in experimental research on the actin cytoskeleton, and experimental data are available that can be used to check the predictions. We first describe the general characteristics of the network, and then calculate the number of connectors and the probabilities of the active configurations involving two connectors. Finally, this information is used to identify the most active contractile configurations from the dependence of the contraction rate.

D1. Characteristics of 2D Circular Networks

In addition to the general hypotheses listed in section A, we consider here that the network occupies a two-dimensional disc of surface S, and is made of F filaments that all have the same length L. For simplicity, we assume that $L \ll \sqrt{S}$, and that filaments are segments of lines positioned randomly within the disc. For a pair of segments forming an angle θ, the probability of them intersecting is $\frac{L^2}{S}\sin\theta$, and the total number of intersections is therefore:

$$X = \frac{F(F-1)L^2}{\pi S}$$

Henceforth, the average number of intersections per filament is $2X/F$. We can thus also calculate the average distance between two adjacent intersections on a filament, denoted L_1, which is the mesh-size of the network:

$$L_1 = \frac{L}{1 + \frac{2X}{F}}$$

The distances between successive intersections are exponentially distributed, with a mean value equal to L_1 (data not shown). Note that the network can be well connected only if this mesh-size is significantly shorter than the filament length ($X > F$).

D2. Number of Connectors in the Network

In this part, we calculate the number of connectors for a given number of Couples in the system, which is the number of Couples that are doubly bound at the intersection points of the network when the binding and unbinding reactions of the Couples have reached equilibrium.

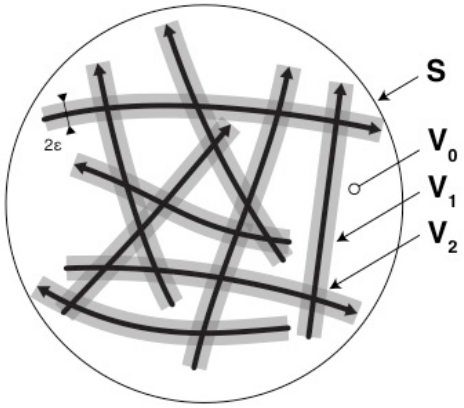

Figure S3: Regions within the network that can capture Couples. The surface area S can be partitioned into three regions: a region V_0 from which a Couple cannot bind, because all filaments are further than the maximum binding distance ε, a region V_1 from which a Couple can bind to one filament, but not to two, and a region V_2 from which a Couple may connect two filaments.

In Cytosim, unbound Couples diffuse freely within the disc that contains the filaments, and we assume that their distribution remains uniform, which should be the case if the associated diffusion constant is high enough. Considering the distance ε at which subunits are able to bind, we partition the surface as follows (Fig. S3): a region V_0 from which binding cannot occur, because there is no filament closer than ε. A region V_1 where binding can lead to a single attachment only, because only one filament is within binding distance ε, and a region V_2 located near an intersection where binding can lead to a connection between two filaments. The size of the three regions can be calculated as $V_2 = 4\pi X\varepsilon^2$ and $V_1 + V_2 = 2FL\varepsilon$, assuming that ε is small such that $2FL\varepsilon \ll S$. To calculate V_2, we integrated over all possible intersection angles. Given these quantities, the binding and unbinding rates (k_{on}, k_{off}), define the transition rates in the state diagram (Fig. S4).

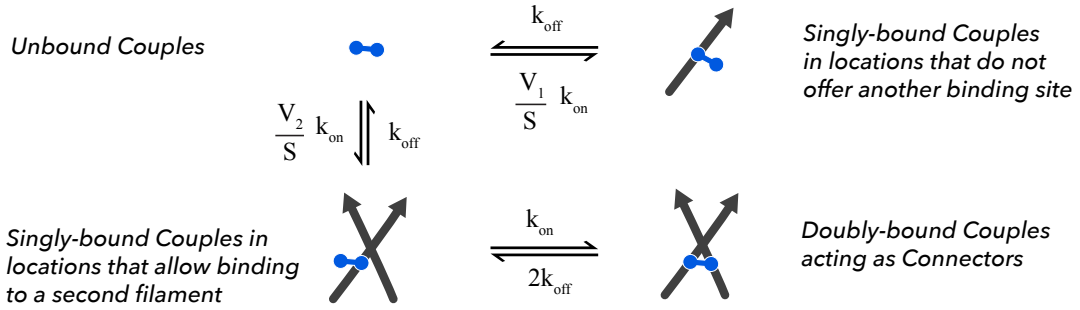

Figure S4: Reaction diagram for Couples within the network. The effective transition rates are defined by the different partitions of the system volume, and the molecular binding and unbinding rates of the activities that make up a Couple.

Finding the equilibrium quantities for such a system (Fig. S4) yields in particular the number of doubly bound Couples, which are the connectors of the network. For example, if the system contains M motor entities, the number of connectors of this type will be:

$$M_2 = M\frac{a^2}{2}\frac{V_2}{S}\left(1 + a\frac{V_1 + V_2}{S} + \frac{a^2}{2}\frac{V_2}{S}\right)^{-1}$$

with

$$a = \frac{k_{on}}{k_{off}}$$

Similarly, we can calculate C_2, the average number of connectors of type crosslinkers, from their number C in the system, and the parameters that determine their binding and unbinding kinetics. These predictions compare well with the results of the stochastic simulation (Fig. S5). Note that for simplicity, we have not considered the active motion of motors in this calculation, and this may account for some of the discrepancy with the simulation results.

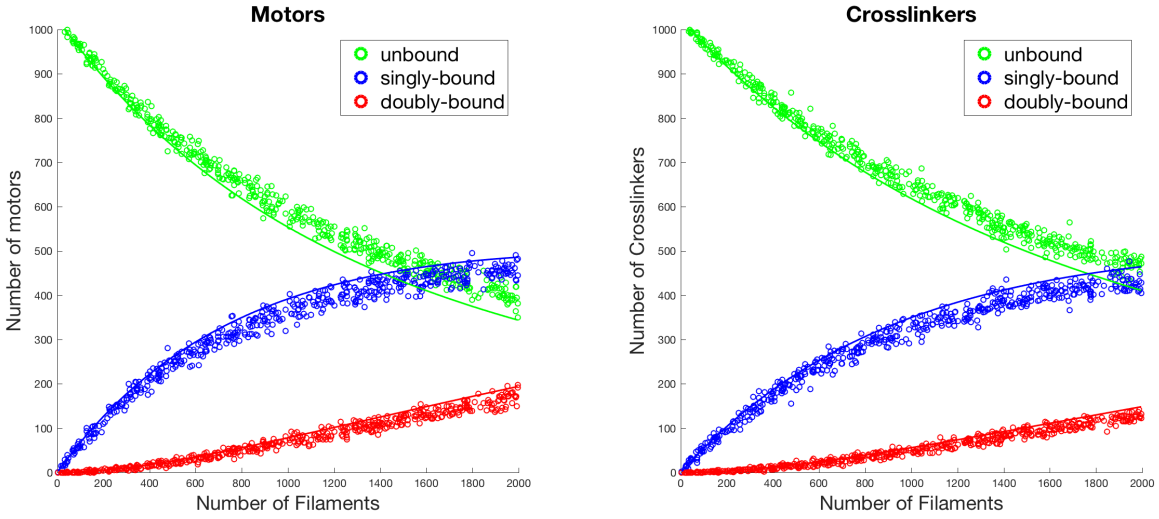

Figure S5: Binding and unbinding of Couples on an immobile network composed of filaments of length 5 μm that are randomly distributed within a disc with a radius of 15 μm. Each dot indicates the result of one simulation in which binding and unbinding was modeled stochastically. The lines indicate the equilibrium quantities predicted by the theory. For this figure, the motors are not motile, since this is meant to only test their binding/unbinding dynamics to filaments. The number of Couples of each type was kept constant at 1024 for all simulations, while the number of filaments was picked randomly between 0 and 2000. The binding rates are 10 s^{-1} and 5 s^{-1} for motors and crosslinkers respectively, their reach is $\varepsilon = 0.01$ μm, and the unbinding rate is 1 s^{-1} for both. We verified that the system had reached equilibrium by comparing the distributions after 100s and 125s.

D3. Number of Connectors per Intersection

The quantities M_2 and C_2 correspond to the average numbers of connectors in the entire network. However, not every intersection in the networks is necessarily occupied by exactly one connector, how the network behaves depends critically on how many intersections are linked by connectors. We therefore now calculate the probabilities of finding zero, one, or more connectors at an intersection. As in the previous section, we will not consider the angle at which filaments intersect and with this simplification we expect the connectors to be distributed uniformly over the intersections. Specifically, the number of connectors of each type on a single intersection is expected to follow a Poisson law, characterized by a single parameter λ (the mean occupancy). The probability of having k connectors at a single intersection is:

$$P(k) = \lambda^k \frac{e^{-\lambda}}{k!}$$

Hence, $P(0) = e^{-\lambda}$ is the probability of having no connector on a particular intersection, $P(1)$ the probability of having exactly one connector, and so on. Motors and crosslinkers will have Poisson laws with different parameters:

$$\lambda_M = \frac{M_2}{X}; \qquad \lambda_C = \frac{C_2}{X}$$

In the following, we will only use two quantities:

$$P_M = 1 - e^{-\lambda_M}; \qquad P_C = 1 - e^{-\lambda_C}$$

P_M and P_C are the probabilities of having one or more connectors of type M or C, at any intersection between two filaments of the network. For our further calculations, we will derive contractility from P_M and P_C only, ignoring the higher order terms of the distributions. This means that we will only take into account whether an intersection has a certain type of connector or not, but we will not distinguish whether it has one or two (or more) motors. This can be expected if the load of the motors is small compared to their stall force, since in this case two motors would move the filaments in the same manner as one. Similarly, we would expect that having one, two or more crosslinkers on one intersection would make little difference, if their stiffness is high enough, which is the case in all our simulations.

The probabilities P_M, P_C, that are within $[0, 1[$, are the likelihood of having one or more connectors of each type. They define the connection density (Fig. S6). If $P_M + P_C < 2$, the number of motors and crosslinkers is not sufficient to bridge every intersection, and many intersections are left unconnected. On the other hand, if the number of connectors is high ($P_M + P_C \approx 2$), most intersections will be connected.

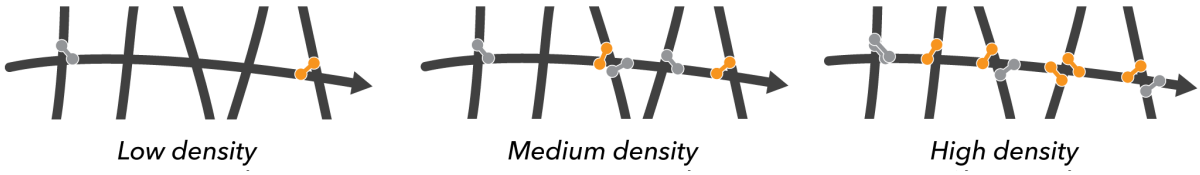

Figure S6: Possible regimes determined by the number of connectors are illustrated here by considering a typical filament in the network. The left diagram depicts a situation in which only few of the intersections are connected ($P_M + P_C < 2$). The diagram on the right depicts a situation in which the number of connectors is high and nearly every intersection point is occupied ($P_M + P_C \approx 2$). The middle diagram depicts an intermediate situation. The number of connectors in the system, which itself depends on the concentration of motors and crosslinkers, their affinity, and the density of filaments will determine in which regime the system is found.

D4. Probabilities of Active Configurations

We make here the inventory of the active configurations involving two connectors that are found in a random network, and calculate their likelihood, given P_M, P_C that were obtained in the previous section. With a mixture of bi-functional motors and bi-functional crosslinkers, only two configurations are associated with a change of distance between the connectors (one expansile and one contractile), but buckling may spoil the force produced by the expansile configuration (Fig. S7).

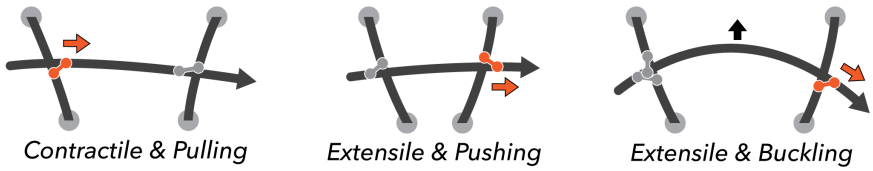

Figure S7: Three configurations and their effects on the network. For each of the diagrams, we focus on one filament that is attached to two other filaments, which are in turn attached to the rest of the network (this is schematically indicated by the gray dots, but the attachment points could be anywhere). The left configuration is contractile, as discussed in the main text, because the red motor is moving towards the arrowhead of the filament, and pulls two filaments closer to each

other. The middle configuration produces an expansile force, provided the filament can sustain the force without buckling. The right configuration could also push on the network, but filament buckling limits the amount of force transmitted to the network. Buckling is more likely on the right configuration than on the middle one, because buckling depends strongly on the distance L, according to: $f_{Euler} = \frac{\pi^2 \kappa}{L^2}$. Thus, increasing the distance L between the two connectors reduces the chance of generating pushing forces.

We assume that one motor (or crosslinker) acts in the same way on one intersection as would two or more motors (or crosslinkers). Nevertheless, the response of the network to the forces generated by the motors depends on the density of connectors per crossing, because this density also determines the distance between successive connectors on a filament, and thus affects the ability of the filament to buckle. To see this more clearly, let us examine systematically the configurations that may arise in a random network. One may find configurations that are either contractile or expansile and where the connectors are more or less distant from each other. Generally, the distance between intersections depends on the mesh size of the network, and we can define this distance as βL_1, where L_1 is the network mesh-size and β is a continuous parameter. In simple terms, $\beta - 1$ is the number of filament intersections located between the two connectors. For any given β, the probabilities of the contractile and expansile configurations are equal, and thus in the absence of buckling, pulling and pushing cancel each other out, producing no net change in network size. However, there exists a threshold β_0 above which buckling spoils the expansile forces, and thus the configurations with $\beta > \beta_0$ can lead to net contraction. This is illustrated in Figure S8, for integer values of β.

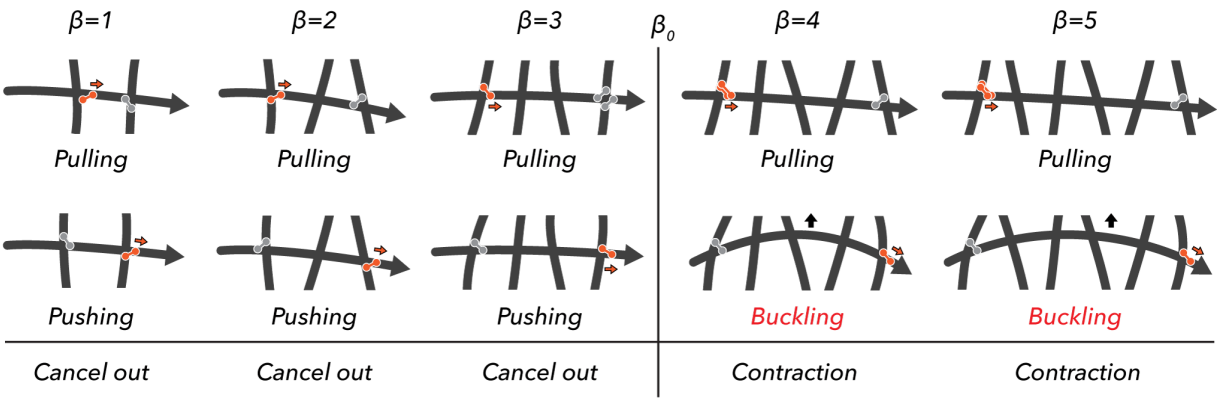

Figure S8: Configurations with two connectors found in a random network. The top row contains pulling configurations, while the bottom row depicts the pushing configurations obtained by swapping motor and crosslinker. The probability of a (top) pulling configuration is thus always equal to the corresponding (bottom) pushing configuration. From left to right, the connectors are positioned increasingly far apart, separated by a distance βL_1, which is a multiple of the network mesh-size L_1. Note that intermediate filament crossings are unconnected, and do not affect the mechanics of the configurations here. However, β determines the likelihood of the configuration, and the buckling force of the filament. For a certain value β_0, the distance $\beta_0 L_1$ permits filament buckling. The value of β_0 depends on filament rigidity and the forces of the motors, and on this illustration, $\beta_0 = 3.5$. For $\beta < \beta_0$, pushing and pulling contributions cancel out. For $\beta > \beta_0$, pulling and pushing do not cancel out since buckling spoils the pushing contributions, leading instead to net contraction.

The likelihood of a configuration in which two connectors are separated by βL_1 is $P_M(1 - P_C)^\beta P_C$, where L_1 is the mesh size and $\beta - 1$ is the number of intermediate unconnected filaments (Fig. S9). Since, with all other things being kept equal, this likelihood decreases with β, shorter

configurations are always more abundant than longer ones. Thus, generally, one would expect the smallest β that allows buckling to correspond to the configuration that has the highest impact on the network.

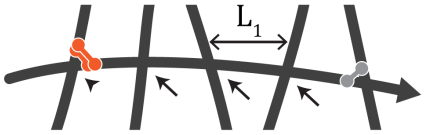

Figure S9: The probability of a configuration depends on its length parameter β, and can be obtained by multiplying the likelihoods associated with each intersection. The first intersection carries a probability $P_M(1-P_C)$ since it should have at least one motor (P_M) and no crosslinker ($1-P_C$). The last intersection on the right carries a probability P_C, since it should have at least one crosslinker, but it may or may not have a motor. By definition of the parameter β, the intermediate intersections indicated with arrows are free of crosslinkers, and if their number is $\beta-1$ (here, $\beta=4$), this occurs with a probability $(1-P_C)^{\beta-1}$. Finally, the entire configuration has a probability $P_M(1-P_C)^{\beta}P_C$. Note that it is not specified if the intermediate positions have a motor or not.

Finally, the threshold β_0 can be estimated from the density of the network, the force of the motors and the bending rigidity of the filaments. We calculate here β_0 such that the force exerted by the motor f_{motor} corresponds to the buckling threshold of the filament over the length βL_1, where L_1 is the mesh size. We thus use $f_{Euler}=\frac{4\pi^2\kappa}{(\beta L_1)^2}$, given the bending rigidity of the filament κ, and assuming that the filament cannot freely rotate at the ends (because it has more connections). This gives a threshold that is 4× higher than for the usual buckling with unconstrained ends. We thus derive:

$$\beta_0=\frac{2\pi}{L_1}\sqrt{\frac{\kappa}{f_{motor}}}$$

This estimate assumes that only one motor is acting at the intersection, which is not always the case. Thus, for high concentrations of motors (P_M close to 1), it may be more appropriate to use a multiple of f_{motor}, which would lead to a smaller value of β. Moreover, if the number of connectors per filament is just above 2, it might be more justified to consider the buckling threshold where the filament is free to pivot: $f_{Euler}=\frac{\pi^2\kappa}{(\beta L_1)^2}$. Despite these potential complications, we find that the value of β for which the best match between prediction and simulation is obtained corresponds to this estimation of β_0.

Figure S10: Zippering configurations contribute to contraction. Here a single intersection is connected with both a crosslinker and a motor (red). If the filaments are sufficiently flexible, or if the angle between the filaments is sufficiently shallow, the motor will be able to move away (red arrow), thereby pulling on the network (black arrows).

While the theory as explained here predicts the major component of the contraction, we found that another configuration also contributes, especially at a high density of crosslinkers. This configuration involves having a motor and a crosslinker on the same intersection, and it produces

contraction in a zipper-like mechanism when the motor moves away from the crosslinker (Fig. S10). The probability of the configuration, which is $P_M P_C$ can be used to improve the fit of the contractile curves. Note that this corresponds to $\beta = 0$ in the general configuration (Fig. S9)

D5. Quantitative Fit of the Contraction Rate

In this part, we analyze the dependence of contraction on the number of crosslinkers and motors by performing simulations. The number of crosslinkers and motors were varied, while all other system parameters were kept constant, yielding results as shown in Fig. S11.

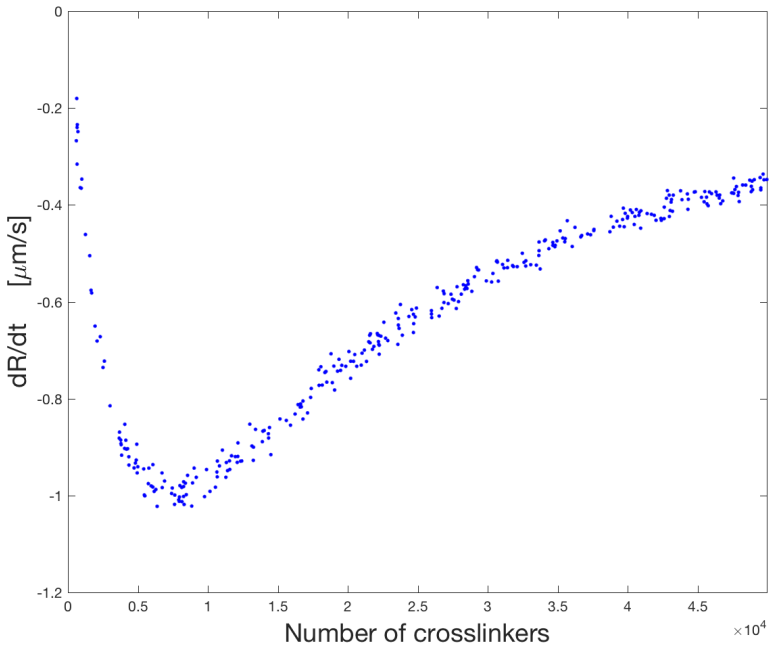

Figure S11: The contractile rate of a network as a function the number of crosslinkers. The number of motors (8000), and all other parameters of the system are kept constant. The area and the contraction rate are calculated as described in Section C. Each dot represents the result of one simulation, for which a new network is chosen randomly.

The net contraction rate of a network depends on several properties such as the speed of the motors, the viscosity of the medium and the viscous drag of the filaments. Even if the viscous drag of one filament is usually negligible compared to the force of a single motor, the cumulative viscous drag of many filaments may become significant. The density of filaments, the size of the network and the type of hydrodynamic interactions between them will thus determine the force required to move the network at a certain rate. Thus, the exact relationship between force and contraction rate can be difficult to predict theoretically. However, we can still analyze here how the contractile rate depends on the number of crosslinkers and motors. For this, we consider two microscopic configurations: the shortest pulling configuration (Fig. S8 & 9) and the zippering configuration (Fig. S10), using their likelihood to fit the network contractility, while P_M and P_C are varied (and fully determined by the parameters of the system). We weight the contributions of the two mechanisms with a parameter α, leading to the fitting function:

$$f = (1-\alpha)P_M P_C + \alpha P_M (1-P_C)^{\beta} P_C$$

The values of α and β are scanned to minimize the sum of the squared residues with the simulation data points. To convert between the dimensionless scalar f and the rate of contraction (μm/s), we used a scaling factor γ, which can be calculated directly. To match a series of simulation data points $\{g_i\}$ with a function f, we used $\{\gamma f_i\}$ with $\gamma = \sum f_i\, g_i / \sum {f_i}^2$, where the $\{f_i\}$ are the values of the function calculated with the parameters used to obtain $\{g_i\}$. This choice of γ minimizes the sum of the squared residues. We then varied systematically the characteristics of the network, such as its size, the number of filaments and their length, and three examples are shown here (Fig. S12 – S14). As a final test of the theory, we compared the value of β for which the best fit is obtained, with the value predicted for β_0.

Figure S12: Example 1 of network contraction

A 2×2μm detail of a network composed of 2000 filaments of length 5μm, contained within a circle of radius 10μm. At this density, there are ~90 intersections per filament. The flexibility of the filament is similar to F-actin (0.05 pN×μm^2).

The predicted exponent is $\beta_0 = 10.43$.

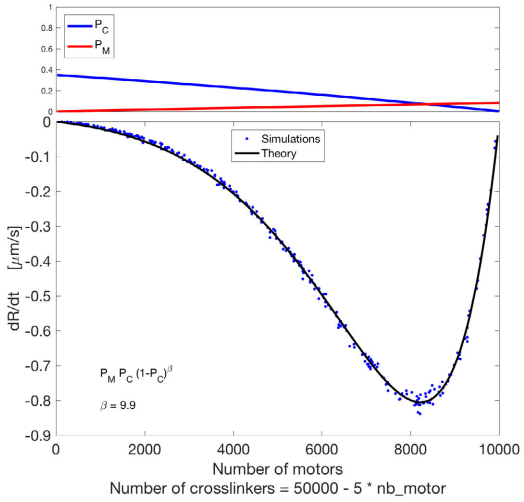

Networks are simulated with varying numbers of crosslinkers, while the number of motors is varied inversely. The resulting contraction rate is fitted by a single probability function associated with the dominant contractile configuration. The best fit is obtained with $\beta = 9.9$. In this case, $\alpha = 1$, as the contribution from zippering (Fig. S10) is not observable.

Figure S13: Example 2 of network contraction

A 2×2μm detail of a network composed of 1000 filaments of length 5μm, contained within a circle of radius 10μm. The flexibility of the filaments is similar to F-actin (0.05 pN×μm^2). At this density, there are ~45 intersections per filament. The predicted exponent is $\beta_0 = 5.27$.

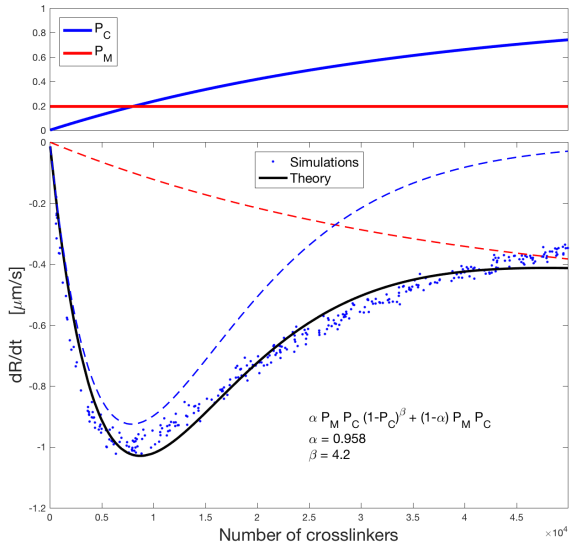

Networks are simulated with varying numbers of crosslinkers, while the number of motors is kept constant at 8000. The resulting variations of the contraction rate are fitted by the probability function describing two contractile configurations. The best fit is obtained with $\beta = 4.2$. The dashed lines indicate the two components of the fitting function.

Figure S14: Example 3 of network contraction

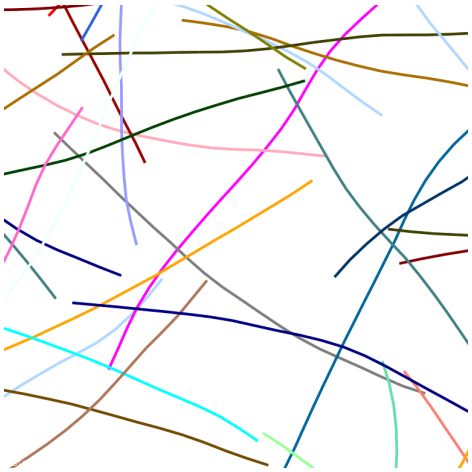

A 2×2μm detail of a network composed of 1000 filaments of length 2μm, contained within a circle of radius 10μm. The flexibility of the filament is similar to F-actin (0.05 pN×μm^2). The density is low, with only ~7 intersections per filament, which is just above the percolation limit. The predicted exponent is $\beta_0 = 2.35$.

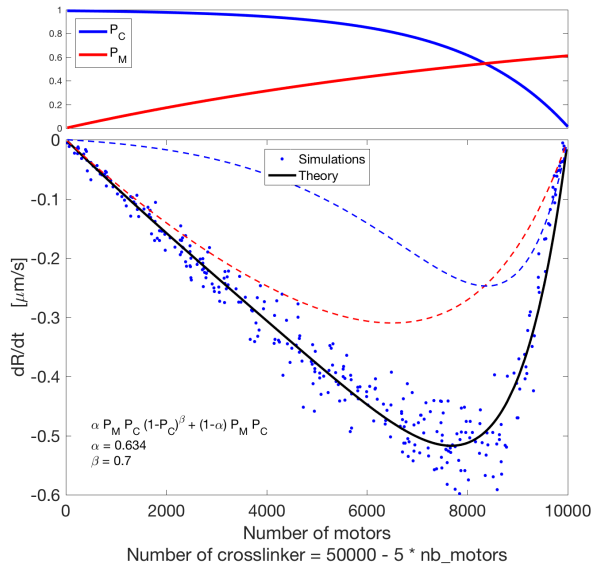

Networks are simulated with varying numbers of crosslinkers, while the number of motors is varied inversely as well. The resulting contraction rate is fitted using the probability functions describing the contractile configurations. The best fit is obtained with $\beta = 0.7$. The dashed lines indicate the two components of the fitting function.

E. Prediction of Contraction Rates for Various Connector Mixtures

The qualitative predictions on the horizontal axis of Fig. 5C are calculated as the weighted sums of all expansile and contractile configurations ($\sum_i p_i v_i$), where p_i is the probability of each configuration to occur and $v_i = \frac{da}{dt}$ is the relative movement of the subunits involved in each configuration. For this figure, we only considered the two limit cases: the regime where filaments are straight and the regime where they buckle under any compressive force. Since all pushing (expansile) configurations have positive values of v_i, while pulling (contractile) configurations have negative values, the sign of the net sum indicates the predicted network outcome (negative, contractile; positive, expansile).

The probability for each configuration was calculated in the same manner as described for the example in the main text for the actin system. For each pair of subunits along a filament we calculate the probability of finding each subunit at a given filament crossing times the probability of not finding a subunit that may cancel the action of the first. For example, a plus-end motor can only be effective if there is not a minus-end motor or a binder subunit (either a general or a minus end-binder) at the same intersection. Thus, a configuration with two opposite motors moving toward each other has the following probability:

$$P_+(1-P_-)(1-P_o)(1-P_m) \times P_-(1-P_+)(1-P_o)\big(1-P_p\big)$$

where P_+, P_-, P_o, P_p and P_m are the probabilities of having at least one plus-end motor, minus-end motor, generic binder, plus-end binder or minus-end binder subunit per filament crossing, respectively; and $1-P$ is the probability of not having that particular subunit. These probabilities are associated with the subunits, and are obtained by summing the connector probabilities calculated as in section D2, taking into account the composition of each connector. For example, a connector composed of two motor (e.g. ++) contributes with a coefficient 1 to the mean occupancy parameter λ_+ used to calculate the probability of its subunits (P_+). A heterogeneous connector composed of different subunits (e.g. +m) contributes with a coefficient $1/2$ to their respective occupancy parameters (λ_+ and λ_m).

F. Prediction of the Contraction/Expansion Rate with End-Binders

When the system contains end-binders, the calculations depicted in section D need to be modified to take into account the fact that end-binders may only bind near one end of the filaments. We derive here the prediction for the network presented on Figure 4, which is plotted with a dashed line on Figure 4D. This 2D network is composed of one kind of plus-end directed motor (+), and two types of end-binders (m, p) from which two types of connectors are made: (+p) and (+m). We first calculate the number of connectors and the probabilities of the active

configurations involving two connectors. From this, we derive the net effects of all configurations, which when negative (resp. positive) predicts a contractile (resp. expansile) behavior.

Given δ, the size of the region near the filament-end (minus- or plus- end) to which an end-binder can attach (Fig. 3D), and following the arguments of section **D1**, the number of intersections occurring near the end of a filament, and at any position of another filament is:

$$X_{\mathrm{p}} = X_{\mathrm{m}} = \frac{F(F-1)}{\pi S} L\delta$$

To calculate the equilibrium number of connectors that bridge two filaments we partition the volume as on Figure S3, replacing X by $X' \in [X_{\mathrm{m}}, X_{\mathrm{p}}]$ and defining $V_2 = 4\pi X'\varepsilon^2$ and $V_1 + V_2 = 2FL\varepsilon$. The binding rate is also modified since the end-binder may not bind to most of V_1, assuming that $\delta \ll F$. The quantities of connectors in the different states are calculated assuming that equilibrium is reached as on Figure S4. Following this approach, we calculate the expected mean number of doubly bound connectors: m_2 and p_2 (both quantities are positive). In the simulation, the number of connectors of each type on a single intersection is expected to follow a Poisson distribution:

$$P(k) = \lambda^k \frac{e^{-\lambda}}{k!}$$

Where $P(k)$ is the probability of having k connectors at a single intersection and λ is a parameter related to the number of doubly bound connectors of each type:

$$\lambda_{\mathrm{m}} = \frac{1}{2}\frac{m_2}{X_{\mathrm{m}}}; \qquad \lambda_{\mathrm{p}} = \frac{1}{2}\frac{p_2}{X_{\mathrm{p}}},$$

from which we derive:

$$P_{\mathrm{m}} = 1 - e^{-\lambda_{\mathrm{m}}}; \qquad P_{\mathrm{p}} = 1 - e^{-\lambda_{\mathrm{p}}}$$

The system has two active configurations, involving one motor and one end binder (Fig. 4A). The likelihoods of these configurations are P_+P_{m} and P_+P_{p}, respectively. Because both connectors in the system involve identical motor subunits, one calculates $P_+ = 1 - e^{-\lambda_+}$ from $\lambda_+ = \frac{1}{2}(m_2 + p_2)/(X_{\mathrm{m}} + X_{\mathrm{p}})$. Finally, the sum of the contributions of all active configurations weighted by the relative subunit movements yields:

$$S = \sum_i v_i p_i = vP_+P_{\mathrm{m}} - vP_+P_{\mathrm{p}} = v(1 - e^{-\lambda_+})(e^{-\lambda_{\mathrm{p}}} - e^{-\lambda_{\mathrm{m}}})$$

The sign of S is determined by the factor $\left(e^{-\lambda_{\mathrm{p}}} - e^{-\lambda_{\mathrm{m}}}\right)$ and predicts whether the system is net contractile or net extensile. The system is extensile if $p_2 = 0$ and contractile if $m_2 = 0$. For the cases where both the minus-end-binder and the plus-end binder subunits have the same binding/unbinding parameters, the system is symmetric, and extensile when the number of (+m) is higher than the number of (+p), neutral if $p_2 = m_2$, and contractile otherwise (Fig. 4D,E).

G. Conclusion

To predict the contraction or the extension of a network, one needs to consider the elementary configurations involving two connectors, and the change in distance between these

connectors. We have done this here in full for a network covering a two-dimensional disc (Section D1). We calculated the likelihood of the active combinations from the properties of the connector subunits (binding rates, etc.). The arguments that we have used are simple and can easily be modified to handle different geometries, or scenarios where the assumptions concerning the binding and unbinding of the motors and crosslinkers would be different.

Our results show that contractility is well fitted by the sum of two curves, which suggests that two types of contractile configurations at most contribute to contractility. A parameter α was used to weight the relative contributions of the two configurations. The value of α can be interpreted as the fraction of contraction due to axial pulling, while the rest is due to zippering. In a dense network (Fig. S12) zippering does not contribute to contraction, and the best fit is obtained for $\alpha = 0$. For sparser networks (Fig. S13) zippering contributes little at low crosslinker density, but may account for the majority of the contraction at high crosslinker density (compare the red dashed line with blue dashed line). The contractility overall is diminished at high crosslinker density, because the likelihood of the axial pulling configuration (Fig. S9) reach zero if $P_C \approx 1$. Finally, for very sparse network (Fig. S14), zippering can account for about half of the contractility.

H. Table of Parameters

This table lists the parameters of the simulation. Whenever possible, we used published, experimentally determined values.

Name	Value	Note
Time step	1 millisecond	Computational parameter. Total time simulated ~ 10s
Viscosity	0.1 pN s/μm²	Effective viscosity of the fluid
k_BT	0.0042 pN μm	Thermal energy at 25°C, defining the Brownian motion of the filaments
Network geometry	R = 15 to 25 μm	Radius of the circular geometry
Filaments		
Filament length	5 μm	[4]
Filament rigidity	0.01 pN μm²	For flexible filaments (Fig. 2) [5]
	0.075 pN μm²	For actin-like system (Fig. 6) [5]
	infinite	Rigid filaments are modelled with only one segment, and may not bend.
Filament segmentation	Between 0.1 and 0.2 μm	Computational parameter
Motor subunits		
Binding	range 10 nm rate 10 s^{-1}	Maximal distance from which a motor can bind to a filament, and rate at which binding can occur
Unbinding	rate 0.3 s^{-1}	Unbinding is independent of load
Motility	Unloaded speed: $v_m = 0.2\ \mu m/s$ Stall force: $f_s = 6\ pN$	The velocity of a motor varies with force $\vec{f}$, as: $v = v_m(1 + \vec{f} \cdot \vec{d}/f_s)$, where $\vec{d}$ is the direction in which the motor would move along the filament if it was unloaded.
Binder subunits		
Binding	range 10 nm rate 10 s^{-1}	Maximal distance from which a binder can bind to a filament, and rate at which binding occurs
Unbinding	rate 0.3 s^{-1}	Unbinding is independent of load
End-binding length	δ = 0.5 μm	Size of region near the plus- or minus-end to which a 'end-binder' may attach
Couples		
Link stiffness	k = 500 pN/μm	Stiffness of the Hookean link between the two subunits of a Couple. If the separation is $\vec{u}$, the force is $\vec{f} = k\vec{u}$
Diffusion	D = 100 μm²/s	

Parameters of Biological Systems

This table lists parameter values measured *in vivo* and *in vitro*.

Name	Value	Reference
Medium viscosity		
Water	0.001 pN s/μm²	7,8
D. melanogaster cytosol	~0.3 pN s/μm²	
C. elegans cytosol	~1 pN s/μm²	
Cleared cytoplasm	0.02 pN s/μm²	
F-Actin		
Length *in vitro*	0–10 μm	4,7
Rigidity	0.075 pN μm²	6,7
Microtubules		
Rigidity	22 pN μm²	3,6
Crosslinkers		
α-actinin unbinding rate	0.37-3.2 s^{-1}	4,9
	0.4 s^{-1}	6,10
	5-15 s^{-1}	11
	0.3-0.4 s^{-1}	12
Filamin unbinding rate	0.6 s^{-1}	10
Fascin unbinding rate	0.12 s^{-1}	13
Myosin		
Binding rate	0.5-1 s^{-1}	14
	6 s^{-1}	15
Unbinding rate	0.18 s^{-1}	16
	13-15 s^{-1}	15
Speed	0.04–1.7 μm/s	17
	0.3 μm/s	16
	0.01–5 μm/s	18
Stall force	2.2 pN	19
	4-12 pN	20
Dynein		
Unbinding rate	0.667 s^{-1}	21,22
Speed	0.8 μm/s	23
Stall force	7-8 pN	23
Kinesin		
Speed	0.6-0.7 μm/s	24
Unbinding rate	0.314 s^{-1}	21,22
Stall force	5-6 pN	24

I. References

1. Purcell, E. M. Life at low Reynolds number. *Am J Phys* **45,** 3–11 (1977).
2. Nedelec, F. & Foethke, D. Collective Langevin dynamics of flexible cytoskeletal fibers. *New Journal of Physics* **9,** 427 (2007).
3. Liu, X. & Pollack, G. H. Mechanics of F-Actin Characterized with Microfabricated Cantilevers. *Biophysical journal* **83,** 2705–2715 (2002).
4. Burlacu, S., Janmey, P. A. & Borejdo, J. Distribution of actin filament lengths measured by fluorescence microscopy. *Am. J. Physiol.* **262,** C569–77 (1992).
5. Gittes, F., Mickey, B., Nettleton, J. & Howard, J. Flexural rigidity of microtubules and actin filaments measured from thermal fluctuations in shape. *J Cell Biol* **120,** 923–934 (1993).
6. Gittes, F., Mickey, B., Nettleton, J. & Howard, J. Flexural rigidity of microtubules and actin filaments measured from thermal fluctuations in shape. *J Cell Biol* **120,** 923–934 (1993).
7. Nedelec, F. & Foethke, D. Collective Langevin dynamics of flexible cytoskeletal fibers. *New Journal of Physics* **9,** 499–510 (2007).
8. Polyakov, O. Y. *Mechanical aspects of Drosophila gastrulation*. (2013).
9. Wachsstock, D. H., Schwartz, W. H. & Pollard, T. D. Affinity of alpha-actinin for actin determines the structure and mechanical properties of actin filament gels. *Biophys J* **65,** 205–214 (1993).
10. Goldmann, W. H. & Isenberg, G. Analysis of filamin and alpha-actinin binding to actin by the stopped flow method. *FEBS Lett* **336,** 408–410 (1993).
11. Miller, B. M., Nyitrai, M., Bernstein, S. I. & Geeves, M. A. Kinetic analysis of Drosophila muscle myosin isoforms suggests a novel mode of mechanochemical coupling. *J Biol Chem* **278,** 50293–50300 (2003).
12. Fritzsche, M., Lewalle, A., Duke, T., Kruse, K. & Charras, G. Analysis of turnover dynamics of the submembranous actin cortex. *Molecular biology of …* (2013).
13. Aratyn, Y. S., Schaus, T. E., Taylor, E. W. & Borisy, G. G. Intrinsic dynamic behavior of fascin in filopodia. *Mol Biol Cell* **18,** 3928–3940 (2007).
14. Rovner, A. S., Fagnant, P. M. & Trybus, K. M. Phosphorylation of a Single Head of Smooth Muscle Myosin Activates the Whole Molecule †. *Biochemistry* **45,** 5280–5289 (2006).
15. Guo, B. & Guilford, W. H. Mechanics of actomyosin bonds in different nucleotide states are tuned to muscle contraction. *Proc Natl Acad Sci USA* **103,** 9844–9849 (2006).
16. Mehta, A. D. *et al.* Myosin-V is a processive actin-based motor. *Nature* **400,** 590–593 (1999).
17. Finer, J. T., Simmons, R. M. & Spudich, J. A. Single myosin molecule mechanics: piconewton forces and nanometre steps. *Nature* (1994).
18. Barua, B., Nagy, A., Sellers, J. R. & Hitchcock-DeGregori, S. E. Regulation of nonmuscle myosin II by tropomyosin. *Biochemistry* **53,** 4015–4024 (2014).
19. Norstrom, M. F., Smithback, P. A. & Rock, R. S. Unconventional processive mechanics of non-muscle myosin IIB. *J Biol Chem* **285,** 26326–26334 (2010).
20. Walcott, S., Warshaw, D. M. & Debold, E. P. Mechanical coupling between myosin molecules causes differences between ensemble and single-molecule measurements. *Biophys J* **103,** 501–510 (2012).
21. Soppina, V., Rai, A. & Mallik, R. Simple non-fluorescent polarity labeling of microtubules for molecular motor assays. *Biotechniques* **46,** 543–549 (2009).
22. Bhat, D. & Gopalakrishnan, M. Effectiveness of a dynein team in a tug of war helped by reduced load sensitivity of detachment: evidence from the study of bidirectional endosome

transport in D. discoideum. *Phys Biol* **9,** 046003 (2012).
23. Toba, S., Watanabe, T. M., Yamaguchi-Okimoto, L., Toyoshima, Y. Y. & Higuchi, H. Overlapping hand-over-hand mechanism of single molecular motility of cytoplasmic dynein. *Proc Natl Acad Sci U S A* **103,** 5741–5745 (2006).
24. Svoboda, K. & Block, S. M. Force and velocity measured for single kinesin molecules. *Cell* **77,** 773–784 (1994).